J Mater Sci (2008) 43:4760–4767
DOI 10.1007/s10853-008-2672-4

Electrical transport properties of $Nd_{0.67-x}Eu_xSr_{0.33}MnO_3$ ($0 \leq x \leq 0.67$) manganites

G. Venkataiah · P. Venugopal Reddy

Received: 9 February 2008 / Accepted: 22 April 2008 / Published online: 20 May 2008

Abstract A systematic investigation of electrical transport properties viz., electrical conductivity and thermopower of Eu-doped Neodymium-based colossal magnetoresistive manganites with compositional formula, $Nd_{0.67-x}Eu_xSr_{0.33}MnO_3$ ($x = 0$–0.67) has been undertaken. These materials were prepared by citrate gel route and characterized by X-ray diffraction, scanning electron microscopy, AC susceptibility, and electrical resistivity measurements. With a view to understand the complex conduction mechanism of these materials, electrical resistivity and thermoelectric power (TEP) data have been analyzed using various theoretical models. It has been concluded that the ferromagnetic metallic part of the conduction mechanism is explained by grain/domain boundary, electron–electron, and magnon scattering mechanisms, while that of high temperature paramagnetic insulating region might be due to small polaron hopping mechanism. The sign change of charge carriers observed in TEP measurements is attributed to the oxygen deficiency of the samples.

Introduction

In recent years, the hole-doped manganites, having the compositional formula, $Re_{1-X}Ae_XMnO_3$ (Re = rare earth ion and Ae = alkaline earth ion) have received considerable attention due to the exhibition of colossal magnetoresistance along with unusual strong coupling among charge, spin, orbit, and lattice degrees of freedom [1]. The substitution of divalent cations (Ca^{2+}, Sr^{2+}, Ba^{2+}, and Pd^{2+}) in the parent insulating compounds, viz., $LaMnO_3$, $PrMnO_3$, $CaMnO_3$, $NdMnO_3$, etc., causes Mn ion to exist in a mixed valence state (Mn^{3+}/Mn^{4+}) [2, 3]. In such manganites, Zener double exchange mechanism [4] comes into play after a certain minimum amount of divalent cation is substituted. This makes manganites to exhibit metal-insulator transition (T_P) and ferromagnetic–paramagnetic transition (T_C) at nearly the same temperature. The main factors that control T_P and T_C are the density of holes created by the divalent cation substitution and the average A-site cation radius ($<r_A>$). In this paper, an effort has been made by keeping the first one (divalent cation substitution) constant and varying the second one systematically. It is clear from the literature that the dramatic changes in electrical transport properties of these manganites can be obtained by doping relatively a smaller trivalent cation such as Eu, Gd, Sm, Y, Dy, etc., at A-site [2, 3]. It has been reported earlier that the MR values of NSMO cannot be increased beyond 40–50% [5]. However, a few reports suggest that MR values can be enhanced considerably when a smaller rare earth ion is doped at A-site. Moreover, substitution of a smaller rare earth ion at A-site also provides the way to understand more and more about local moments of charge carriers, which are responsible for thermo emf [6].

Among various transport properties, thermopower is a simple and sensitive one for analyzing the charge carrier dynamics [7]. Therefore, the phenomenon of thermopower has attracted the attention of several investigators [8–13]. In fact, a systematic analysis of thermopower data also enables one to understand the conduction mechanism. In

G. Venkataiah · P. Venugopal Reddy (✉)
Department of Physics, Osmania University,
Hyderabad 500 007, India
e-mail: pvenugopalreddy@yahoo.com

G. Venkataiah
Department of Physics, National Cheng Kung University,
Tainan 701, Taiwan, ROC

view of theses facts, a systematic investigation electrical transport properties of Eu substituted NSMO manganites has been investigated and the results of such an investigation are presented here.

Experimental details

A series of polycrystalline materials with the compositional formula, $Nd_{0.67-x}Eu_xSr_{0.33}MnO_3$ ($x = 0$, 0.07, 0.17, 0.27, 0.37, 0.47, 0.57, and 0.67), was prepared by the sol–gel method [14] by sintering at 1,200 °C. The X-ray diffraction (XRD) measurements were carried out on a Phillips (Xpert) diffractometer with Cu K_α radiation, while the scanning electron microscopy measurements were performed on Philips FEIXL30 ESEM microscope. AC susceptibility measurements were performed using a dual channel lock-in-amplifier (Stanford Research Systems, Model SR530), while the electrical resistivity and magnetoresistance measurements were carried out using a JANI'S 'super-varitemp' cryostat in magnetic fields of 3 and 7 T, over a temperature range 10–300 K.

Finally, two probe differential methods were employed for the measurement of thermoelectric power (TEP) over a temperature range 77–300 K. In this technique, silver-coated samples are placed between two copper electrodes and suitable facilities are available in the sample holder to maintain appropriate temperature gradient. The measurements were carried out in nitrogen atmosphere (exchange gas) in the heating mode. Finally, the measured thermopower data were corrected subtracting thermopower values of copper to get the absolute thermopower values of the samples.

Results and discussion

XRD and SEM measurements

The X-ray diffraction measurements of all the samples have been carried out at room temperature and the data were analyzed using Rietveld refinement technique (see Fig. 1) [15]. The refined crystallographic data of all the samples are given in Table 1. It is clear from the analysis that the samples are having single-phase, without any detectable impurity. The variation of lattice parameters with increasing Eu-concentration is not systematic, while the unit cell volume is decreasing (see Table 1). The average crystallite size of the materials has been estimated using peak broadening technique [16]. In this process, SiO_2 is used to correct the intrinsic width associated with the equipment. The calculated average crystallite size values ($<S>$) are in the range, 135–215 nm and are given in Table 2.

The SEM measurements of all the materials were undertaken and are shown in Fig. 2. It is clear from the figure that the average grain size values are found to be in the range 0.4–1.8 μm and that the grain size values are increasing with increasing Eu-concentration.

In order to evaluate the oxygen stoichiometry of the samples, iodometric titrations [17] were carried out and the results are included in Table 2. It can be seen from the table that the oxygen deficiency is increasing with increasing Eu-content in the materials. Further, the oxygen deficiency of the first four samples (Eu-0 to Eu-3) is less when compared with the remaining four samples of the series. In general, the oxygen deficiency is expected to introduce point defects and lattice distortions, which in turn may act as trapping centers for the charge carriers. Therefore, the oxygen vacancies present in these materials might have affected the magnetic and transport properties considerably resulting in the reduction of Mn^{4+} concentration.

Magnetic and electrical

With a view to understand the variation of magnetic and electrical transition temperatures (T_C and T_P) with Eu-concentration, AC susceptibility, and electrical resistivity measurements were undertaken over a temperature range 77–300 K. Figure 3 shows the variation electrical resistivity with temperature for all the samples. Ferro to paramagnetic transition temperatures (T_C) and metal insulator transition temperature (T_P) were determined from the inflection point of $d\chi/dT$ versus temperature and $d\rho/dT$ versus temperature curves, respectively, and are given in Table 2. In order to explain the variation of both these transition temperatures with dopant concentration, the average A-site cation radius ($<r_A>$) and A-site cation mismatch quantifying parameter ($\sigma^2 = \Sigma y_i r_i^2 - <r_A>^2$) have been calculated and are given in Table 2. It can be seen from the table that σ^2 values are increasing continuously with increasing Eu-content. It is clear from Table 2 that the values of T_P and T_C are decreasing with increasing Eu-concentration. The details of magnetic, electrical, and magnetoresistance studies on these samples are given in an earlier publication published from this laboratory [16].

Thermoelectric power

TEP measurements of all the samples of the present investigation have been carried out over a temperature range 77–300 K. The Seebeck coefficient values (S) were evaluated and their variation with temperature is shown in Fig. 4. It is clear from S vs. T plots that Eu-0, Eu-1& Eu-2 samples are showing a peak in the vicinity of Curie temperature (T_C), while the other samples, Eu-3 to Eu-7, show

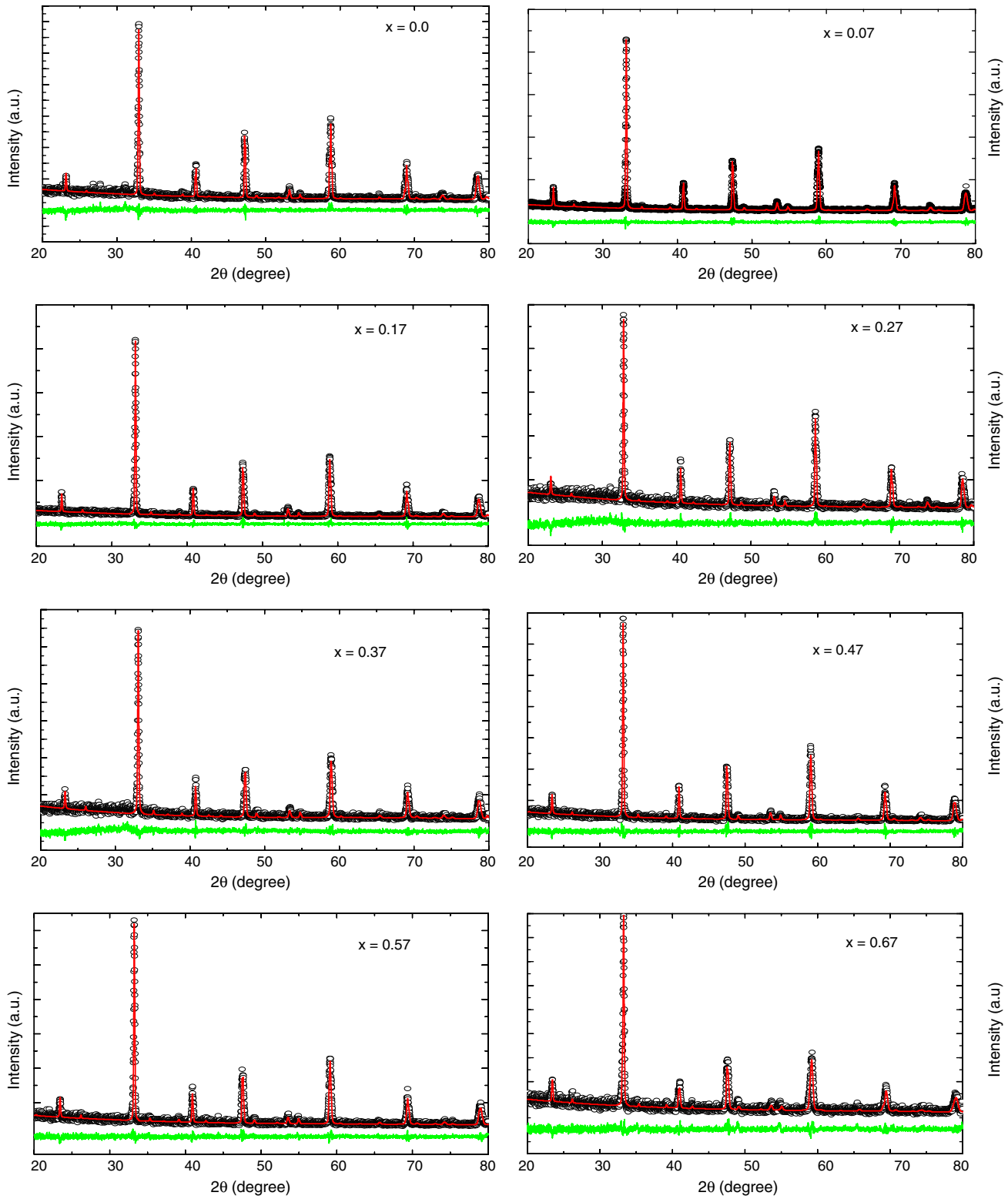

Fig. 1 X-ray diffraction patterns of $Nd_{0.67-x}Eu_xSr_{0.33}MnO_3$ ($0 \leq x \leq 0.67$) manganites, observed pattern is shown with dots, calculated profile using Rietveld method is shown as solid line, and the pattern given below is the difference of both

a valley. The values of transition temperature (T_S) were evaluated from the inflection point of dS/dT versus T plots and are given in Table 2. It is clear from the table that T_S values are found to be high when compared with T_P and T_C values. The reason for the observed high T_S values (except in the case of Eu-0 and Eu-3 samples) may be due to

Table 1 Crystallographic data of $Nd_{0.67-x}Eu_xSr_{0.33}MnO_3$ manganites

x		0	0.07	0.17	0.27	0.37	0.47	0.57	0.67
Sample code		Eu-0	Eu-1	Eu-2	Eu-3	Eu-4	Eu-5	Eu-6	Eu-7
a (Å)		5.4671	5.4654	5.4595	5.4529	5.4493	5.4508	5.4495	5.4583
b (Å)		5.4447	5.4472	5.4477	5.4459	5.4424	5.4426	5.4377	5.4264
c (Å)		7.6965	7.6984	7.6981	7.6877	7.6943	7.6813	7.6769	7.6670
Volume (Å^3)		229.10	229.19	228.95	228.30	228.19	227.88	227.49	227.09
Nd/Eu/Sr (0.67/0.33)	x	0.9970	0.9975	0.9962	0.9950	0.9996	0.9979	0.9942	0.9998
	y	0.0203	0.0216	0.0285	0.0225	0.0236	0.0248	0.0261	0.0266
O (1)	x	0.0383	0.0442	0.0838	0.0634	0.0917	0.0339	0.0447	0.0195
	y	0.4978	0.4878	0.5009	0.4957	0.4767	0.4999	0.4926	0.4895
O (2)	x	0.7258	0.7217	0.6866	0.7134	0.7220	0.7162	0.7137	0.7199
	y	0.2589	0.2654	0.2429	0.2792	0.2833	0.2639	0.2618	0.2681
	z	0.0478	0.0420	0.0138	0.0090	0.0094	0.0476	0.0485	0.0590
R_P (%)		17.79	16.53	17.12	20.04	17.80	17.59	17.84	17.91
R_{WP} (%)		24.82	24.83	24.64	26.21	24.37	25.06	24.77	24.56
R_{exp} (%)		21.90	22.08	22.21	21.68	21.50	22.35	22.50	22.28
Goodness-of-fit		1.13	1.12	1.11	1.21	1.13	1.12	1.10	1.10

The atoms are located at the following Wyckoff positions Nd (Eu and Sr) 4(c):(x, y, 1/4); Mn 4(b): (1/2,0,0); O(1) 4(c):(x, y, 1/4) and O(2) 8(d):(x, y, z)

Table 2 Experimental data of $Nd_{0.67-x}Eu_xSr_{0.33}MnO_3$ ($x = 0.0$–0.67) manganites

Sample code	<S> (nm)	T_C (K)	T_P (K)	T_S (K)	r_A (Å)	σ^2 (Å^2)	Oxygen concentration
Eu-0	150	265	264	265	1.212	0.0048	2.999
Eu-1	215	241	242	250	1.209	0.0052	2.997
Eu-2	210	211	206	232	1.204	0.0057	2.994
Eu-3	140	175	176	176	1.199	0.0063	2.992
Eu-4	135	128	116	158	1.196	0.0068	2.979
Eu-5	140	114	84	154	1.191	0.0072	2.978
Eu-6	150	–	84	150	1.187	0.0076	2.979
Eu-7	180	–	86	146	1.183	0.0080	2.967

electronic inhomogenities present in the samples, which arises mainly due to magnetic clusters. It is well known that this behavior is attributed to the large size mismatch between A-site cations or large σ^2 [18] Further, as the transport phenomena are correlated with magnetism in these systems, the ferromagnetic interaction between these clusters leads to delocalization of the carriers, which in turn might lower thermopower even before T_C is reached leading to a fall in the values of thermo power in the vicinity of T_S. This may lead to a higher value of T_S than T_C. At very low temperatures, S value drops sharply with decreasing temperature (i.e., $S \rightarrow 0$ as $T \rightarrow 0$), which is nearly independent of the doping level.

It is also clear that Eu-0 to Eu-3 samples are found to exhibit positive S values through out the temperature range of investigation, while the samples Eu-4 to Eu-6 are exhibiting both negative and positive signs. Finally, Eu-7 sample is found to exhibit only negative S values throughout the temperature range of investigation. Therefore, one may conclude from S versus temperature plots that there exist two different types of carriers in these manganites. The positive sign exhibited by Eu-0 to Eu-3 might be attributed to the holes which are excited from the valence band into the impurity band, while in the case of Eu-4 to Eu-6 samples, the change in sign may be attributed to the large oxygen deficiency present in the sample [19]. It is well known that the oxygen environment influence the crystal field splitting thereby affecting spin–orbital degree of the freedom of charge carriers. Therefore, there is a possibility to change of sign from negative to positive with varying Eu content.

Conduction mechanism

In order to understand the complex conduction mechanism and the relative strengths of various scattering mechanisms at low temperature (i.e., in the temperature range 10 K to

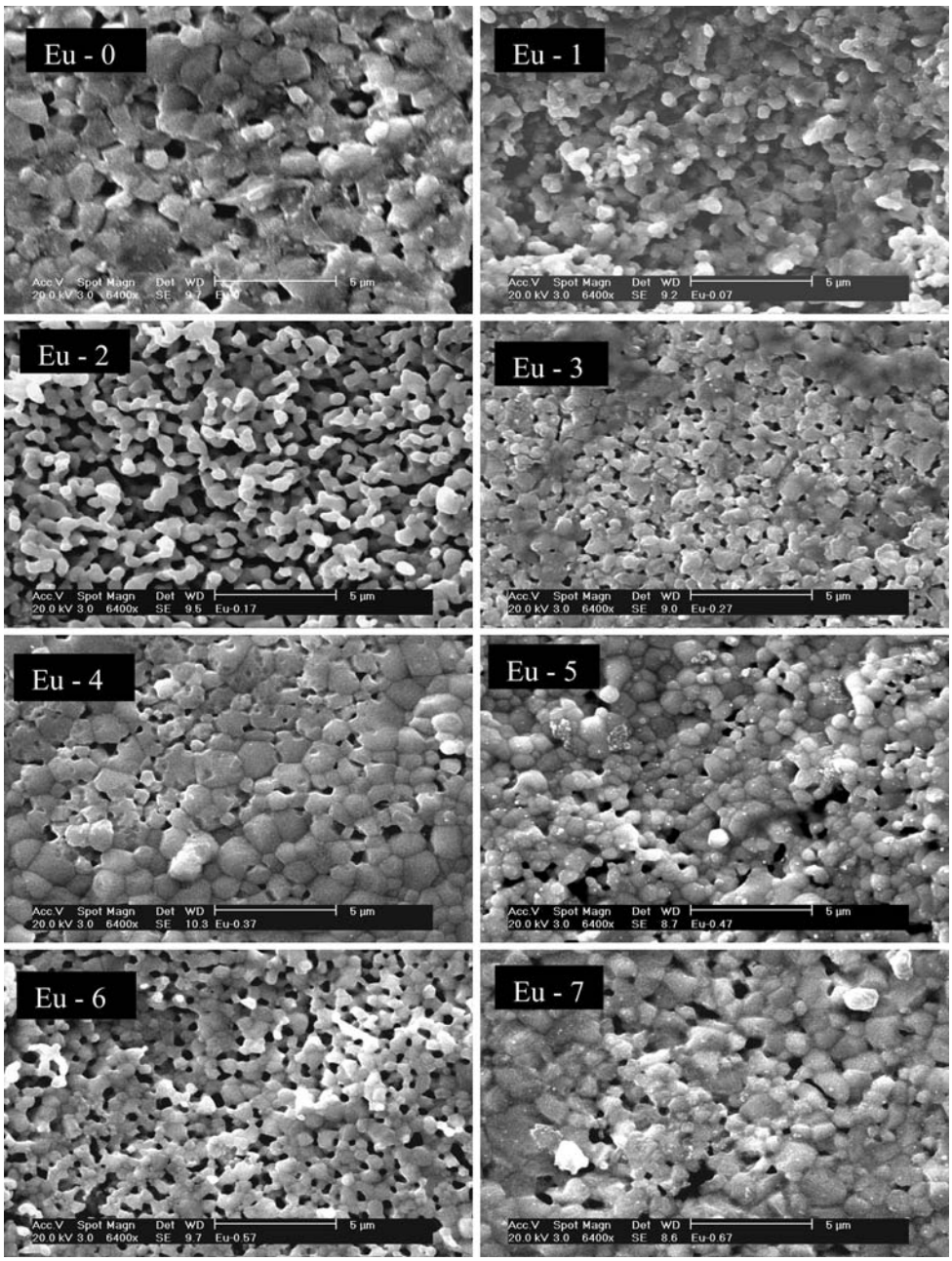

Fig. 2 SEM images of $Nd_{0.67-x}Eu_xSr_{0.33}MnO_3$ ($0 \leq x \leq 0.67$) manganites

T_P, except in the case of Eu-6(0T)), an attempt has been made to fit the resistivity data to various empirical equations [20–22].

$$\rho = \rho_0 + \rho_2 T^2, \tag{1}$$

$$\rho = \rho_0 + \rho_{2.5} T^{2.5}, \tag{2}$$

$$\rho = \rho_0 + \rho_2 T^2 + \rho_{4.5} T^{4.5}. \tag{3}$$

In the above equations, ρ_0 term arises due to the grain/domain boundary [21, 22]. On the other hand, $\rho_2 T^2$ term in Eqs. 1 and 3 represents the resistivity due to electron–electron scattering process [20, 23], while the term $\rho_{2.5} T^{2.5}$ represents resistivity due to single magnon scattering process in ferromagnetic phase [20, 22, 24]. Finally, the term $\rho_{4.5} T^{4.5}$ is attributed to two magnon scattering process in the ferromagnetic region [22]. Actually, it is assumed that the later process is more favorable in half-metallic band structure materials such as manganites.

The quality of these fittings is evaluated by comparing the square of linear correlation coefficient (R^2). One can note from R^2 values that the equation, $\rho(T) = \rho_0 + \rho_2 T^2 + \rho_{4.5} T^{4.5}$ is found to fit well with the experimental data and the best-fit curves in the case of Eu-2 and Eu-6 are shown in Fig. 5. A close examination of the fitting data and experimental observations, it has been concluded that the transport mechanism in manganites of the present

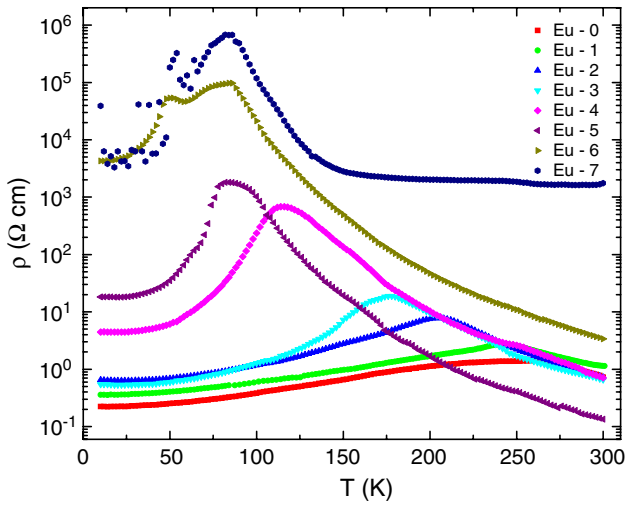

Fig. 3 Variation of electrical resistivity with temperature of $Nd_{0.67-x}Eu_xSr_{0.33}MnO_3$ ($0 \leq x \leq 0.67$) manganites

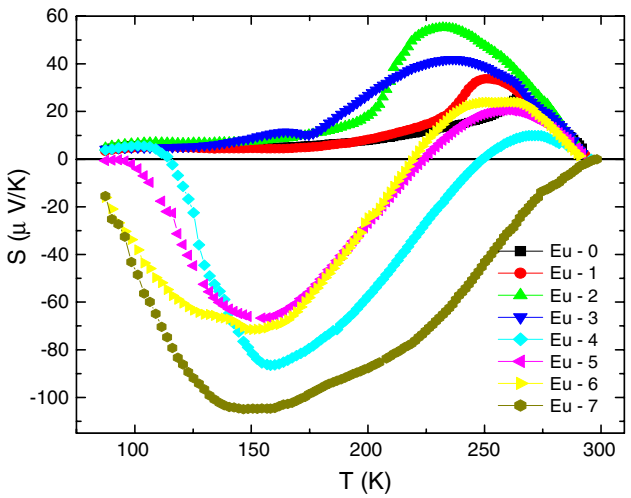

Fig. 4 Variation of thermoelectric power with temperature of $Nd_{0.67-x}Eu_xSr_{0.33}MnO_3$ ($0 \leq x \leq 0.67$) manganites

investigation, in the low temperature region ($T < T_P$) may be attributed to the grain/domain boundary, electron–electron, and magnon scattering mechanisms, thereby indicating that the metallic region lies in the FM phase.

It is interesting to note from the analysis of the transport data that ρ_0 values are increasing continuously with increasing Eu content, implying that Eu doping might have resulted in the enhancement of domain or grain boundary scattering. In contrast, the other two parameters (ρ_2 and $\rho_{4.5}$) are found to vary irregularly. However, all the three parameters (ρ_0, ρ_2, and $\rho_{4.5}$) are found to decrease with the increasing magnetic field and the observed behavior may be due to enlargement of the magnetic domain. This in turn

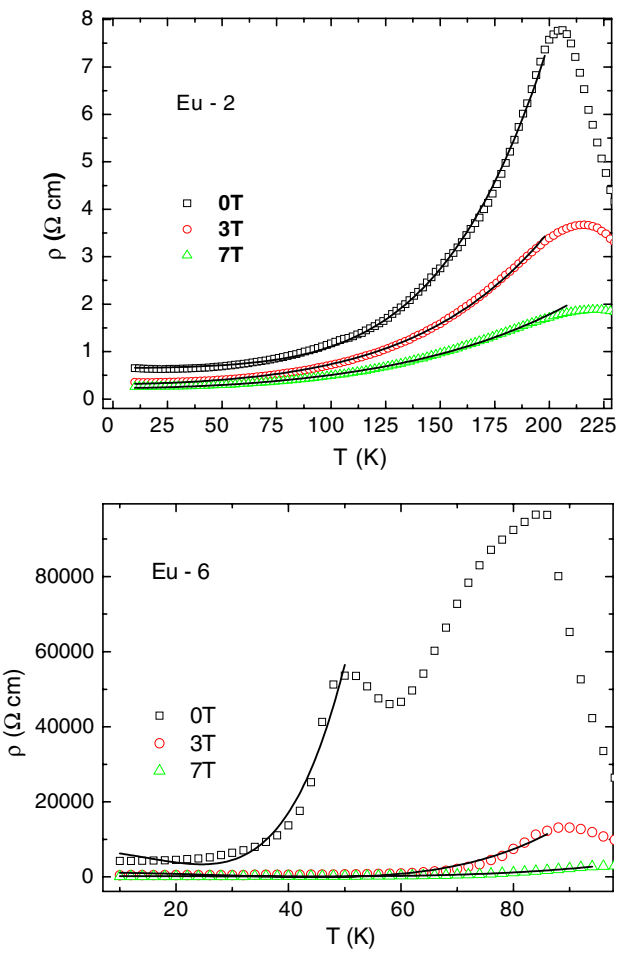

Fig. 5 Plots of ρ versus temperature in the case of Eu-2 and Eu-6 samples both in presence and absence of magnetic field. The solid line gives the best-fit to the equation $\rho = \rho_0 + \rho_2 T^2 + \rho_{4.5} T^{4.5}$

suppresses various scattering effects due to parallel configuration of the spins in the domain.

The high temperature ($T > T_P$) electrical resistivity has been fitted to the two different models in different temperature regions. In order to explain the electrical conduction just above T_P, i.e., $T_P < T < \theta_D/2$, (θ_D is Debye's temperature) variable range hopping (VRH) model [25] has been used, while adiabatic small polaron hopping (SPH) model [26] is considered at temperatures beyond $\theta_D/2$. Typical plots corresponding to these models are shown in Figs. 6 and 7, respectively.

From the fitting parameters of VRH model, the values of density of states at the Fermi level, $N(E_F)$ have been estimated and are found to be in agreement with the reported ones [5, 14, 21]. The values of $N(E_F)$ are higher in the presence of the field and this may be due to the suppression of magnetic domain scattering with the application of the field [5]. Further, in the temperature region, $T > \theta_D/2$, the resistivity data have been fitted to SPH model and from the fitting parameters, activation energies (E_P) have been

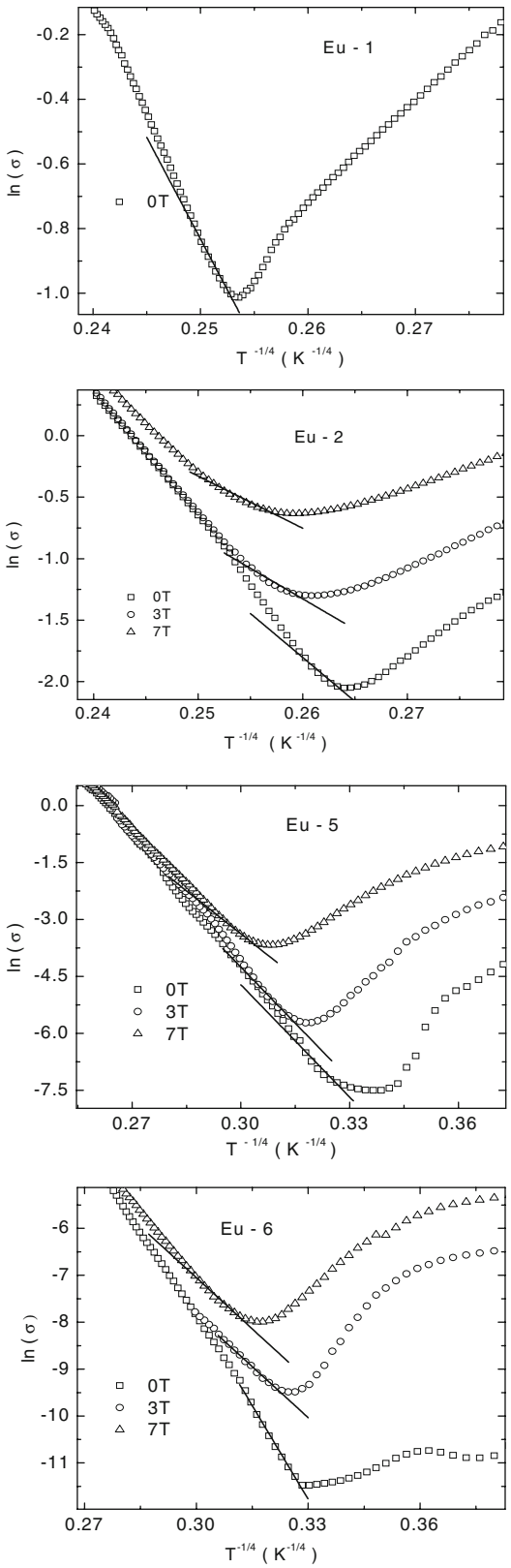

Fig. 6 Plots of ln(σ) versus $T^{-1/4}$ in the case of Eu-1, 2, 5, and 6 samples. The solid line indicates the best-fit for VRH model

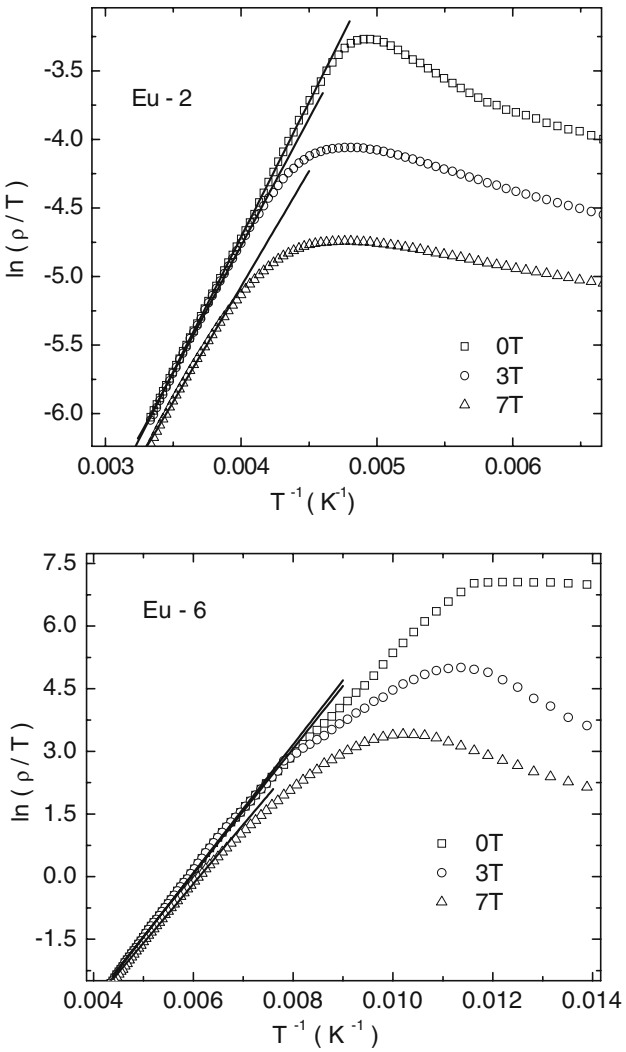

Fig. 7 Plots of ln(ρ/T) versus T^{-1} in the case of Eu-2 and Eu-6 samples. The solid line indicates the best-fit for SPH model

estimated and are found to be in the range of 120–170 meV, which in agreement with the values reported earlier [14, 20]. It is interesting to note that E_P values are decreasing with increasing magnetic field and the observed behavior may be due to the localization of charge carriers in the presence of magnetic field [27].

Conclusions

In conclusion, the nature of the charge carriers is found to change from hole-like character to electron-like character with increasing Eu content in the material. The electrical conduction mechanism at low temperatures ($T < T_P$) can be explained based on electron–electron and two magnon scattering processes, while the adiabatic SPH and VRH

mechanisms are used to explain the variation of resistivity in the high temperature ($T > T_P$) regions.

Acknowledgements One of the authors (G. Venkataiah) is grateful to CSIR, Govt. of India for awarding Research Associate (RA) Fellowship.

References

1. Jin S, Tiefel TH, McCormack M, Fastnacht RA, Ramesh R, Chen LH (1994) Science 264:413
2. Rao CNR, Raveau B (eds) (1998) Colossal magnetoresistance, charge ordering and other related properties of rare earth manganates. World Scientific, Singapore
3. Ramirez AP (1997) J Phys Condens Matter 9:8171
4. Zener C (1951) Phys Rev 82:403
5. Venkataiah G, Venugopal Reddy P (2005) J Magn Magn Mater 285:343
6. Chen B, Uher C, Morelli DT, Mantese JV, Mance AM, Micheli AL (1996) Phys Rev B 53:5094
7. Blatt FJ, Schroeder PA, Foiles CL, Greig D (1976) Thermoelectric power of metals. Plenum, New York
8. Fisher B, Patlagan L, Reisner GM, Knizhnik A (1997) Phys Rev B 55:9227
9. Yamada S, Amira T, Ikeda H, Takita K (2000) J Phys Soc Japan 69:1278
10. Tomioka Y, Asamitsu A, Kuwahara H, Moritomo Y, Tokura Y (1996) Phys Rev B 53:R1689
11. Yoshizawa H, Kawano H, Tomioka Y, Tokura Y (1995) Phys Rev B 52:R13145
12. Rao CNR, Cheetham AK (1997) Science 276:911
13. Mandal P (2000) Phys Rev B 61:14675
14. Venkataiah G, Venugopal Reddy P (2005) Solid State Commun 136:114
15. Young RA (1993) The Rietveld method. Oxford University Press, New York
16. Venkataiah G, Prasad V, Venugopal Reddy P (2007) Solid State Commun 141:73
17. Vogel AI (1978) A text book of quantitative inorganic analysis including elementary instrumental analysis, 4th edn. Longman, London
18. Kundu AK, Nordblad P, Rao CNR (2006) J Phys Condens Matter 18:4809
19. Taskin AA, Lavrov AN, Ando Y (2006) Phys Rev B 73:121101
20. Benerjee A, Pal S, Chaudhuri BK (2001) J Chem Phys 115:1550
21. Snyder GJ, Hiskers R, DiCarolis S, Beasley MR, Geballe TH (1996) Phys Rev B 53:14434
22. De Teresa JM, Ibarra MR, Blasco J, García J, Marquina C, Algarabel PA, Arnold Z, Kamenev K, Ritter C, von Helmolt R (1996) Phys Rev B 54:1187
23. Urushibara A, Moritomo Y, Arima T, Asamitsu A, Kido G, Tokura Y (1995) Phys Rev B 51:14103
24. Pi L, Zhang L, Zhang Y (2000) Phys Rev B 61:8917
25. Mott NF, Davis EA (1971) Electronic process in noncrystalline materials. Clarendon, Oxford
26. Emin D, Holstein T (1969) Ann Phys 53:439
27. Bhattacharya S, Mukherjee RK, Chaudhuri BK (2003) Appl Phys Lett 82:4101